Journal of the European Ceramic Society 36 (2016) 2535–2542

Contents lists available at www.sciencedirect.com

Journal of the European Ceramic Society

journal homepage: www.elsevier.com/locate/jeurceramsoc

Flash sintering of alumina: Effect of different operating conditions on densification

Mattia Biesuz[a,*], Vincenzo M. Sglavo[a,b]

[a] Department of Industrial Engineering, University of Trento, Via Sommarive 9, 38050 Trento, Italy
[b] INSTM Research Unit, Via G. Giusti 9, 50121 Firenze, Italy

ARTICLE INFO

Article history:
Received 27 February 2016
Received in revised form 16 March 2016
Accepted 17 March 2016
Available online 22 March 2016

Keywords:
Flash sintering
Alumina
Joule heating
Conduction
Activation energy

ABSTRACT

Nearly pure α-alumina samples produced by uniaxial pressing were flash sintered under electrical fields ranging from 500 V/cm to 1500 V/cm in experiments at constant heating rate. Sintering temperature significantly decreased with the applied E-field even down to ≈900 °C at 1500 V/cm. The onset temperature for flash sintering can be successfully modelled as a function of the applied voltage. The sintering temperature is also shown to be strongly affected by the electrode materials used during the treatment: using silver or carbon electrodes the sintering temperature is about 300 °C lower than when using platinum electrodes. In addition, the bulk density and porosity of the sintered alumina ceramic correlate strongly with the imposed current limit. Power dissipation was analysed before and during flash sintering; the activation energy for conduction was calculated in both cases, indicating that the process is based on ionic diffusion phenomena. Finally, we showed that during flash sintering the activation energy for conduction decreases, suggesting the occurrence of physical or structural modifications induced by current localization at the grain boundaries.

1. Introduction

The reduction of environmental, energetic and economic costs is today of major concern to the ceramic industry. Several recent studies [1–19] have shown that the application of an electrical field is very effective in reducing sintering time and temperature and so also energy consumption and CO_2 emissions. In particular, at specific electrical field and temperature levels, so called flash sintering (FS) can be observed [1–19]. This phenomenon, which is accompanied by an abrupt increase in material conductivity, can reduce the sintering time to a few seconds and typically allows densification of ceramics at temperatures much lower than conventional. This sintering technique has been studied in many high temperature ionic conductor (YSZ [1–8], GDC [9]), protonic conductor ($BaCe_{0.8}Gd_{0.2}O_{3-d}$ [10]), semi-conductors (SiC [11]), composites (ZrO_2-Al_2O_3 [12,13], CAS glass—Al_2O_3 [14]) and electrically conductive ($MnCo_2O_4$ [15,16], LSCF [17,18]) ceramics.

Although there are various phenomenological explanations proposed for describing this unusual behaviour, the mechanisms leading to material densification are still unknown. Some proposed mechanisms involve local heating at the grain boundaries [1,19] or the formation of Frenkel pairs [19,20] driven by the applied electrical field. Also Joule heating was suggested as responsible for the rapid densification; nevertheless, some experimental results have shown that the sample surface temperature is far lower than would be needed for conventional sintering in a few seconds [3,20]. Recently, Todd et al. developed a model indicating that a thermal runaway of Joule heating can induce an FS event [4]. Similar results were also independently obtained by Zhang et al. [21]. Todd also suggested that the temperature in the sample core upon FS can be much higher than that measured on the surface, although stating that "*the mechanistic details of densification remain uncertain*". The problem is anyway still open and controversial.

Although FS has been demonstrated in several semi-conductive and conductive ceramics, very little work has been done on resistive materials. Cologna et al. made some experiments on high purity alumina and concluded that this could not be flash sintered. It was also shown that alumina completely changes its electrical behaviour if doped with 0.25 wt% MgO; and MgO-doped alumina was successfully flash sintered down to 1260 °C [19].

In this work, we subjected 99.8% pure alumina to flash-sintering experiments in order to understand the possible conduction mechanisms and the densification behaviour in a widely used resistive oxide ceramic. We also intended to observe the influence of some

* Corresponding author.
E-mail address: mattia.biesuz@unitn.it (M. Biesuz).

http://dx.doi.org/10.1016/j.jeurceramsoc.2016.03.021
0955-2219/

operating conditions on FS, such as electrical field intensity, current density and electrode materials.

2. Experimental procedure

In this work we used nearly pure α-Alumina (Almatis, CT 3000 SG, d_{50} = 0.6 μm, d_{90} = 3.0 μm) with nominal composition Al_2O_3 99.8 wt%—MgO 0.04 wt%—Na_2O 0.03 wt%—Fe_2O_3 0.015 wt%—SiO_2 0.015 wt%—CaO 0.015 wt%. After adding 6 wt% distilled water, dog bone samples were produced by uniaxial pressing at 120 MPa. The thinner cross section of the pressed sample was 3 mm × 3.3–4 mm. Sintering tests were carried out in a Linseis L75 dilatometer with a constant heating rate of 20 °C/min. We applied a DC field, using a Glassman EW series 5 kV–120 mA power supply, when the sample reached 350 °C and this was maintained at constant value until the current limit was reached. The field and the current density ranged from 250 to 1500 V/cm and from 2 to 7 mA/mm^2, respectively. We measured the current intensity and the voltage at 1 Hz using a multimeter (Keithley 2100). On reaching the current limit, we maintained the current flow for 2 min and then shut down the system.

The power supply connections to the samples were two platinum wires, forced into holes on opposite edges of the dog bone sample. To improve the electrical contact between these platinum electrodes and the ceramic, we used various conductive pastes. The first type, used for most experiments, was platinum-based (Sigma Aldrich). We also used silver paste (Agar Scientific) and carbon cement (Plano GMBH) for comparison.

The density of the sintered samples was measured by Archimedes' method using a balance (Gibertini) with sensitivity ±0.1 mg. Only the constant-cross section part of the specimen between the two electrodes was used for the density measurements.

3. Results and discussion

3.1. Effect of current, voltage and electrode material

Fig. 1 shows the effect of the electrical field on the sintering behaviour of alumina for samples with platinum electrodes. First, we see immediately that the material considered can be flash sintered under an electric field (E-Field) in excess of 500 V/cm; if a voltage of 250 V/cm is applied, the shrinkage is limited.

The sintering temperature decreases significantly at higher E-fields, up to 1500 V/cm, when the material sinters at around 920 °C. This shows clearly an anticipated sintering process if compared to the results collected by Cologna et al. on 0.25 wt% MgO-doped alumina [19]: the onset temperature for flash sintering (FS), in fact, decreases by 120–230 °C (under the same field). This anticipated sintering process cannot be related to the different grain size [5], the powder we used being coarser (d_{50} = 0.6 μm, d_{90} = 3.0 μm) than that used by Cologna et al. (100–300 nm). In addition, we noted that the MgO-doped alumina used by Cologna et al. contains a larger amount of impurities (0.25 wt%) if compared with the material used here (0.20 wt%). This suggests that the anticipated FS phenomenon could be explained by some beneficial effect on corundum conductivity associated with the simultaneous presence of different chemical elements. Several authors have reported very limited cationic solubility in corundum [22–24], the solubility of magnesia at 1720–1880 °C being only 75–175 ppm [24]. This means that almost all MgO contained in the powder used in the present work (and also in that used by Cologna et al.) produces the precipitation of a second resistive phase (periclase), which is not very effective for increasing the material conductivity. If different chemical elements are simultaneously added in amount larger than their solubility

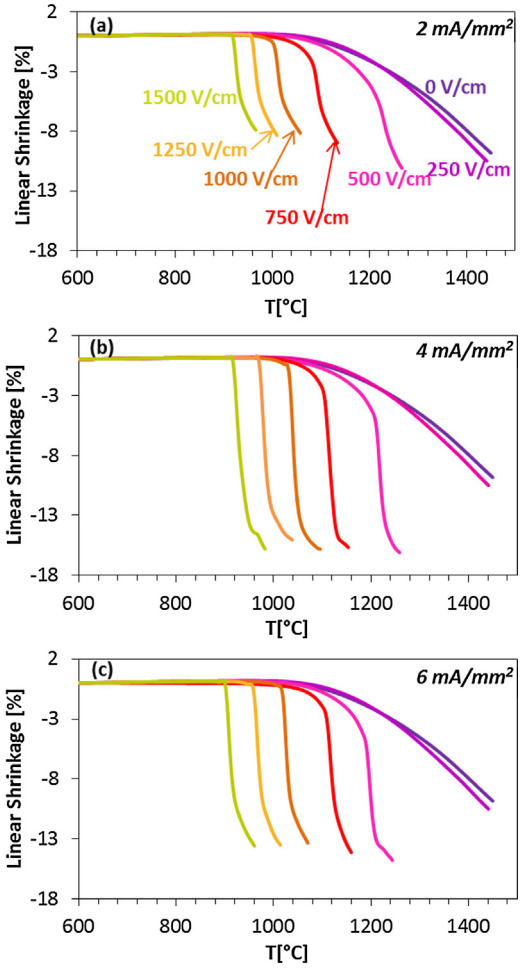

Fig. 1. Shrinkage curve for alumina sintered using Pt electrodes at various voltages and with nominal current densities of 2 mA/mm^2 (a), 4 mA/mm^2 (b) and 6 mA/mm^2 (c).

limit in alumina, it is reasonable to assume that the total amount of Al^{3+} that can be substituted by the doping cations is higher than what would be obtained by adding only MgO. In this solid solution, elements with oxidation number lower than 3 (e.g., Mg^{++} or Ca^{++}) act as electron acceptors [25,26] and promote the formation of oxygen vacancies [26–28]; conversely, elements with oxidation number larger than 3 (like Si^{4+}) behave as donors [25,26] and promote the formation of aluminium vacancies, as previously reported [28]. In this way, both ionic and electronic conductivity increase as a result of both greater vacancy concentration and narrower band gaps for electrons to jump in the conduction band, respectively.

Samples tested under low voltage (500–750 V/cm) exhibit two different densification mechanisms. The first occurs before reaching the current limit and is responsible for 3–6% linear shrinkage. The dilatometric plots show a characteristic downward concavity. The densification in this case is partially due to "conventional/thermal" sintering mechanisms. Nevertheless, we see that shrinkage increases with the applied E-Field: therefore, an electrical contribution to densification is also clearly present. For this reason, this sintering mechanism can be defined as Field Assisted Sintering (FAS).

The second part of the sintering process is characterized by an upward concavity in the dilatometric plots, occurring just after reaching the current limit. This is properly called flash sintering.

The samples tested under high voltage (1000–1500 V/cm), sinter at temperatures lower than 1050 °C and therefore FS is responsible

for almost all the densification. In this case, the linear shrinkage upon sintering appears almost independent of the applied voltage.

Based on Fig. 1, we note that the final shrinkage and the sintering rate (the slope of the dilatometric plot) increase with the nominal current density. Some other physical properties of the sintered bodies, such as apparent porosity and bulk density (Fig. 2), also improve if a more intense current is applied. In fact, it is possible to achieve a large decrease of open porosity by increasing the current from 2 to 4–5 mA/mm^2. At a higher current, a plateau is reached with no further significant advantage. Therefore, the nominal current density is always the key parameter controlling the sintering rate and the final density of ceramic bodies. This is probably due to the higher specific power dissipation levels, obtained by increasing the current limit (as will be shown in the following Section 3.2 below).

Fig. 2 shows two different trends. The first regards the sample sintered under low voltage (500 V/cm and partially 750 V/cm). As explained before, the densification phenomena in such samples already partially activate when the current limit is reached. It is possible to see that the material is almost fully dense with only 4 mA/mm^2 nominal current density and also that the specimens sintered at 2 mA/mm^2 are characterized by limited open porosity (∼7%). Conversely, the specimens tested under E-Field in excess of 1000 V/cm are characterized by high apparent porosity (>20%) and limited density (<3.1 g/cm^3) when sintered at 2 mA/mm^2. These specimens reach complete densification only at 5–6 mA/mm^2.

Fig. 3 shows the specific power dissipation as a function of the furnace temperature. Two different regions can be identified: the first, at power dissipation less than 25 mW/mm^2, is characterized by FAS; the second shows instead an abrupt increase in power dissipation and FS occurs. This deviation from the normal linear-like behaviour, which is accompanied by a drop in material resistivity, was observed by many authors [1,2,9,13] usually in the power range 1–15 mW/mm^3. Various reasons were proposed to explain this behaviour and among these, the most discussed are local grain boundary heating [1,19], Frenkel pair formation [19,20] and Joule heating (although some experimental results pointed out that this is not the fundamental densification mechanism [3,20]).

Even in the FAS region, the behaviour of the system is not perfectly linear, i.e. the slope of the curve increases slightly with 1/T. This behaviour may be caused by various conduction mechanisms, that with the highest activation energy appearing only at high temperature [29–32]. Moreover, it should not be forgotten that the specimen undergoes several modifications during heating (i.e. neck formation provides a continuous and interconnected path for current flow) which can lead to an increase in conductivity.

In any case, quasi-linear behaviour provides a good approximation of the power dissipation plot in the region before FS. The activation energy for the conduction mechanism was therefore calculated by interpolating the experimental data over a 250 °C temperature range, before deviation from linearity due to FS (as is shown for example in Fig. 3 for a sample treated under 1500 V/cm); the calculation was made considering the plots recorded by using different electrode materials. The activation energy was estimated as 1.2 ± 0.2, 1.2 ± 0.1, 1.0 ± 0.2 eV for platinum, carbon and silver electrodes, respectively. Similar results were found by Cologna et al. (1.5–2.3 eV) [19], Pan et al. (1.5–2.4 eV) [29], Mohapatra and Kroger (2–2.1 eV) [33] and Öijerholm et al. (1 eV) [34] who worked with dense alumina bodies. The calculated activation energies are far lower than the band gap for pure corundum (8.7–10.8 eV) [36–39]. The presence of the grain boundary (more "disordered" material) can only partially account for a narrower band gap: for example, values around 3.2–8.7 eV are reported for amorphous alumina [37,38,40], still far larger than those estimated here.

The presence of aliovalent atoms can also alter the difference between conduction and valence bands; for example, magnesium can act as electron acceptor or silicon as electron donor [25,26]. Research described in the literature shows the band gap evolution to be a function of the doping elements; nevertheless, band gap energies around 4–5 eV are reported [38,39], still larger than the results previously reported.

Although partial electronic contribution to conduction cannot be completely excluded, it does not seem to be the main conduction mechanism. Some clear findings support this hypothesis. In fact, it is reported that electronic conduction in alumina is activated at high temperature, becoming predominant around 1400 °C [29,41–44]. Other authors suggest that conduction is still ionic, and based on Al^{3+} diffusion, even at high temperature (1000–1650 °C) [35].

The problem of diffusion in corundum is very controversial and very large data scatter is found for oxygen and aluminium self-diffusion. Heuer has produced the most complete work summarizing current knowledge of this topic [45]. He reported several experimental data showing that, in most cases, the measured activation energy for lattice self-diffusion in alumina is in the range 3–8 eV. These measurements were often carried out using a radiotracer at high temperature (>1300 °C). In addition, the work showed that the grain boundary presence does not reduce these values enough to make them comparable with the conduction activation energy, as determined in Refs. [45–47].

On the other hand, other experiments were carried out at lower temperature (usually <1200 °C) by electrical tests (i.e. EIS, interfacial polarization) fixing the energy barrier for Al and O self-diffusion in the range 0.8–2.4 eV [29,34,43,48]. Such values are in agreement with those found in this study and perfectly match with those (0.7 and 2.5 eV) obtained by theoretical calculation [26,27,49,50].

Some explanations can be proposed to account for the observed differences:

i At high temperature, diffusion paths with higher energy barriers are activated [29–32]. It was shown that a transition between intrinsic and extrinsic diffusion can be observed at around 1600–1650 °C [30,31]. At lower temperature, diffusion is "*impurity-controlled*" or "*structure-sensitive*" [30] or is concentrated through fast paths, as at dislocations. Oishi et al. showed that in crushed alumina the activation energy for oxygen diffusion is reduced to 1.87 eV as a result of the high concentration of line defects [51].

ii Some surface effect on diffusion cannot be excluded *a priori*. Öijerholm and Pan pointed out that the activation energy for oxygen surface diffusion in corundum should be around 1 eV although even in this case a large scatter is reported [52,53].

iii Finally, one should consider that the presence of different point defects with net charge leads to the formation of clusters by electrostatic interaction. This phenomenon is well-known in doped alumina [26–28,50]. In particular, clusters binding Mg'_{Al} and VÖ were extensively studied and binding energies in the range 1.3–3.5 eV were calculated. Therefore, as was suggested by Tewari [27], when the activation energy for diffusion is measured, the contribution of clusters cannot be neglected. Tewari estimated that the Mg^{++} presence leads to an increased energy barrier for VÖ diffusion of 2–3 eV, this accounting for the difference between calculated and activation energy measured by radiotracer. We can also say that the activation energies measured by the electrical method [29,34,43,48] are in good agreement with the theoretical values [26,27,49,50] and with those we found. This can be accounted for by the fact that clusters are broken by the E-Field application and, once broken, the rapid movement of vacancies can inhibit their reformation.

Fig. 4 shows the sintering temperature as a function of the E-Field when different electrode materials are used. We can see that by changing the electrode the system also alters its response upon

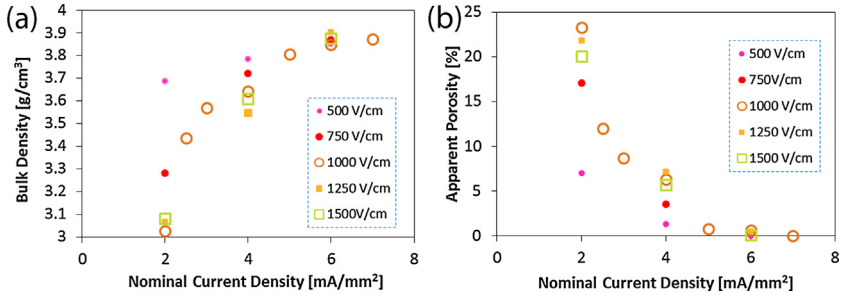

Fig. 2. Bulk density (a) and apparent porosity (b) of alumina sintered between Pt electrodes as a function of the nominal current density.

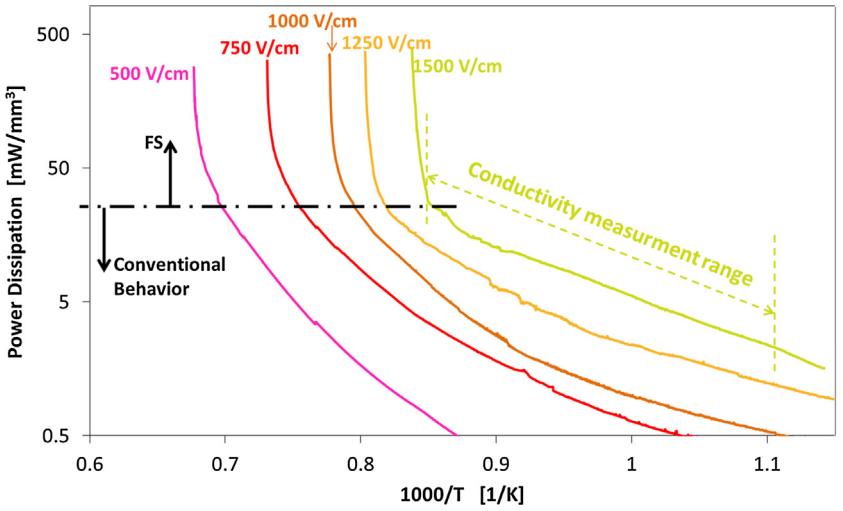

Fig. 3. Specific power dissipation during FS experiments (current limit = 600 mA/mm^2). The dashed line indicates the temperature range used for activation energy measurement in the sample treated under 1500 V/cm.

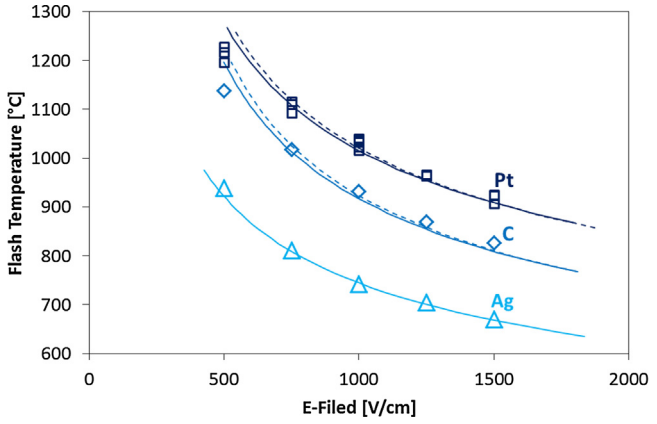

Fig. 4. Onset temperature for FS as a function of the applied E-Field. The continuous curves represent the interpolating function; the dashed lines are the interpolating curves calculated removing the point at 500 V/cm.

sintering. In particular, by adding silver paste, the onset sintering temperature is reduced by about 250 °C with respect to the use of platinum electrodes. The carbon cement determines behaviour more similar to Pt paste although the samples are sintered at lower temperature. The improvement of electrode contacts, accompanied by a resistance decrease, does not seem to be a reasonable justification for such a large difference. It seems that carbon and especially silver somehow catalyse reactions at the alumina/metal electrode interface, increasing the conductivity of the system. Conversely, platinum, being a noble metal, does not produce any interaction.

The carbon cement remains stable during the runway upon FS as demonstrated by thermal analyses which indicate that the used paste is substantially inert up to 1200 °C. One can speculate that a variation in the oxidation state of carbon promotes the formation of defects in Al_2O_3; i.e., crystal defects such as oxygen vacancies can be produced in alumina by a combined effect of anodic polarization and carbon oxidation leading to increased conductivity.

The presence of silver can also enhance the conductivity in three ways:

i It is extensively reported that the Ag^+ diffusion coefficient in corundum is much higher than the self-diffusion coefficients for aluminium and oxygen [54,55]. This suggests a conduction mechanism where silver ions are the main charge carriers. Nevertheless, we found no evidence of silver presence as detected by EDS in the central part of the dog bone sample used here. Moreover, the differences in the activation energies for Ag/C and Pt electrodes are not high enough to state that different conduction mechanisms are activated.

ii Silver, being a monovalent ion, when substituting an aluminium ion can promote the formation of crystal defects (as reported for other aliovalent species [25–28]). The result is an increased defect population, with enhanced conductivity.

iii Silver and platinum possess different work function, it being lower in Ag (4.52–4.74 eV [56,57]) than in Pt (5.12–5.93 eV [56,57]). In other words, the charge carriers have to overcome lower potential at the metal/ceramic interface nears the electrode and this can partially account for the observed behaviour.

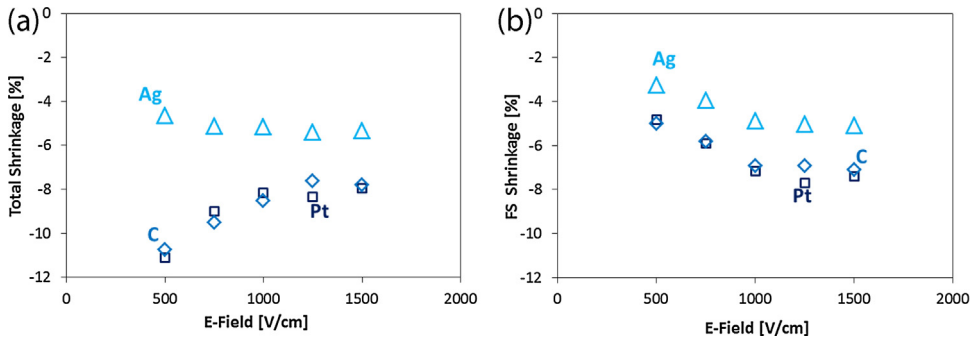

Fig. 5. Total linear shrinkage upon sintering (a) and shrinkage obtained during the Flash Sintering event (b) for different electrode materials (current limit = 2 mA/mm^2).

The experimental data, relating the E-Field and the onset temperature for FS, were fitted by a recursive method using the model developed by Todd et al. [4] for isothermal FS experiments. The model is based on a power balance between the electrical power and the heat dissipated by radiation. The equations relating the onset furnace temperature for FS and the applied electrical field are:

$$\frac{E^2V}{\rho_0}exp\left(\frac{-Q}{R\left(T_f+\Delta T\right)}\right)=S\sigma\varepsilon\left(\left(T_f+\Delta T\right)^4-{T_f}^4\right) \quad (1)$$

$$\frac{E^2V}{\rho_0}\frac{Q}{R\left(T_f+\Delta T\right)^2}exp\left(\frac{-Q}{R\left(T_f+\Delta T\right)}\right)=4S\sigma\varepsilon\left(T_f+\Delta T\right)^3 \quad (2)$$

where E is the E-Field, Q and ρ_0 the activation energy and the pre-exponential constant of the resistivity respectively, T_f the furnace temperature, ΔT the sample overheat needed for FS, σ the Stefan-Boltzmann constant, ε the emissivity, R the universal gas constant, V and S the volume and the surface of the sample, respectively. Eq. (2) can also read:

$$E^2=\frac{4S\sigma\varepsilon R\rho_0}{V}\frac{\left(T_f+\Delta T\right)^5}{Q}exp\left(\frac{Q}{R\left(T_f+\Delta T\right)}\right)$$

$$=A\frac{\left(T_f+\Delta T\right)^5}{Q}exp\left(\frac{Q}{R\left(T_f+\Delta T\right)}\right) \quad (3)$$

where A is a constant. By combining Eqs. (1) and (2) a relationship between the sample temperature needed for FS and the furnace temperature can be obtained:

$$\frac{4R}{Q}{T_s}^5-{T_s}^4+{T_f}^4=0 \quad (4)$$

where $T_s = T_f + \Delta T$. The application of this model to the given constant-heating rate FS is an approximation. In fact, we assumed that the time needed for sample heating is always zero but this is not true since the sample has its own heat capacity. This is responsible for a delay in the FS events with respect to the model. Moreover, the sample temperature cannot be homogeneous (the surface is always colder due to irradiative heat exchange). Nevertheless, it is possible to hypothesize (also because of the very limited sample sizes) that this delay is not significant and, in any case, a similar delay is present in all samples.

The experimental data interpolation was recursive, as follows:

i The activation energy (Q) is assumed equal to 50 kJ/mol;
ii Using Eq. (4) and the experimental results for the onset furnace temperature (T_f), T_s was calculated for each sample by NSolve command in Mathematica®;

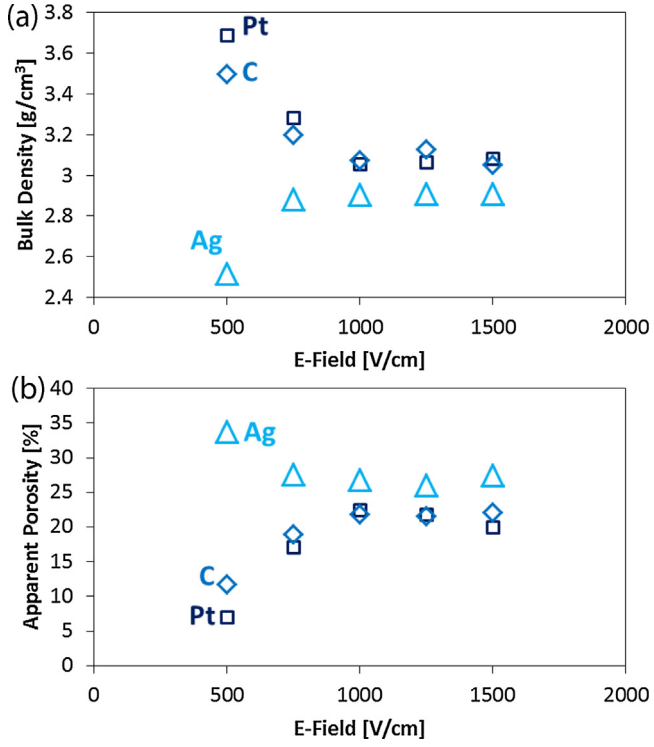

Fig. 6. Bulk density (a) and apparent porosity (b) of samples flash sintered using different electrode materials at various voltages (2 mA/mm^2).

iii A new value for Q and for the constant A was estimated by Eq. (3) using FindFit function in Mathematica®;
iv With the new Q value, all the operations were repeated until Q changes less than 0.05 kJ/mol between two successive iterations.

The best fit was found using activation energies of 1.57, 1.37 and 1.32 eV for platinum, carbon and silver electrodes, respectively. These values are similar to those previously calculated from the slope of the power dissipation plots. As shown in Fig. 4, the model provides a good approximation of the experimental results in the case of Pt and C electrodes, and the error is nearly negligible (always lower than 17 °C) if Ag electrodes are used. The experimental data, which do not appear perfectly fitted by the model, are those taken at 500 V/cm, especially for Pt and C electrodes; in this case, the samples are flash sintered at temperature lower than that expected by the model. This is probably due to material properties changing when heated, the specimens treated under limited voltage being already partially sintered when FS occurs. In this way a continuous path forms for current flow, leading to a decrease in resistivity and anticipating FS. The data fitting obtained excluding the data at

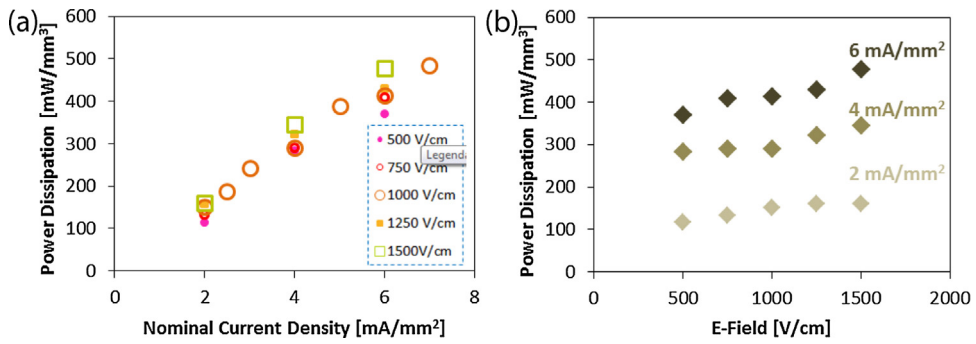

Fig. 7. Average specific power dissipation during FS as a function of current density (a) and applied E-Field (b) using platinum electrodes.

500 V/cm gives activation energies of 1.53 and 1.34 eV for Pt and C electrodes, respectively, close to those previously calculated.

In any case, one can undoubtedly point out that the model provides satisfactory fitting of the experimental data also for constant-heating rate FS experiments. The results are consistent and supported by the previous activation energy calculations.

The electrode material also has an important effect on alumina densification. The total shrinkage upon sintering and the shrinkage after reaching the current limit and FS occurrence, are reported in Fig. 5. We see that the material tested using Pt and C electrodes behaves similarly, while the samples sintered using Ag paste show much lower shrinkage. This result is also supported by the density and porosity measurements (Fig. 6), which clearly indicate that the specimens treated using silver electrodes are less dense and more porous. When Pt and C electrodes are used, the only difference (as shown in Fig. 6) regards the samples treated under limited voltage (500–750 V/cm). In such cases, FAS—thermal sintering cannot be neglected. Therefore, it is not surprising that the samples sintered with Pt electrodes are denser than the others, due to the higher sintering temperature.

The specimens treated using silver electrodes have characteristic lower density and shrinkage and larger open porosity. In this case, the samples were always sintered at temperature lower than 950 °C and, therefore, the densification is mainly due to FS. The sample treated under low voltage (500 V/cm) is less dense than the others, although treated with the same current density and flash sintered at higher temperature. We can relate the reasons for the different densification behaviour, to the combination of power dissipation and furnace temperature or to the activation of different conduction mechanisms. However, current experimental evidence does not support the second hypothesis (the activation energy being similar for all the considered systems).

3.2. Power dissipation during flash sintering

Fig. 7 shows the average specific power dissipation during FS when using Pt electrodes. The reported values take into account the sample size evolution upon sintering, using the hypothesis of isotropic shrinkage. One can immediately observe that, in the tested condition, power dissipation is substantially proportional to the electrical current, J. This means that the system is not ohmic upon FS, i.e. it does not follow the second order relation:

$$P = \rho_{(T)} J^2 \tag{5}$$

where P is the specific power dissipation, $\rho_{(T)}$ the resistivity and J the current density. Therefore, we can assume that the resistivity decreases with J. This should not be surprising since the system is working at higher temperature by imposing higher J.

The effect of the applied electrical field on power dissipation is less evident. Nevertheless, we see a slight increase of power dissipation at higher E. This is probably connected to the different

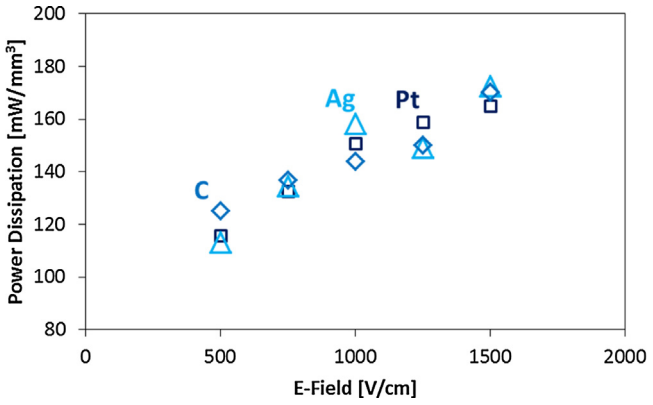

Fig. 8. Average specific power dissipation during FS as a function of the applied E-Field for different electrode materials (2 mA/mm²).

FS temperature: in fact, by increasing the field, the specimen is flash sintered at lower temperature, thus decreasing the sample temperature and conductivity. The result is increasing electrical power.

The different electrode materials do not significantly affect power dissipation (Fig. 8). This is probably the result of two different aspects. First, the samples sintered at low temperature (Ag) should be colder and more resistive; then, such specimens shrink less leading to lower specific power densities. Probably these two phenomena balance each other.

We modelled the resistivity data, collected using platinum electrodes, via the exponential equation:

$$\rho = \rho_0 \exp\left(\frac{Q}{RT_s}\right) \tag{6}$$

where ρ_0 is a pre-exponential constant, Q the activation energy for the conduction mechanism and T_s the sample temperature. T_s can be estimated, under the approximation that heat is completely transmitted by radiation, as:

$$T_S = \left(T_f^4 + \frac{PV}{\sigma\varepsilon S}\right)^{1/4} \tag{7}$$

where T_f is the furnace temperature, V and S the specimen volume and surface, respectively, σ the Stefan-Boltzmann constant and ε the emissivity.

Only the data collected 1 min after the beginning of flash sintering were interpolated: this is done to ensure that the specimens were at a reasonably constant temperature and to avoid errors due to sample evolution upon sintering. The best fit of the data was found using an emissivity of 0.65 and activation energy of 0.94 eV. These results are still not compatible with electronic conduction. The estimated value for ρ_0 during FS was 0.0316 Ωm, much higher than that calculated from the slope of the power dissipation curve

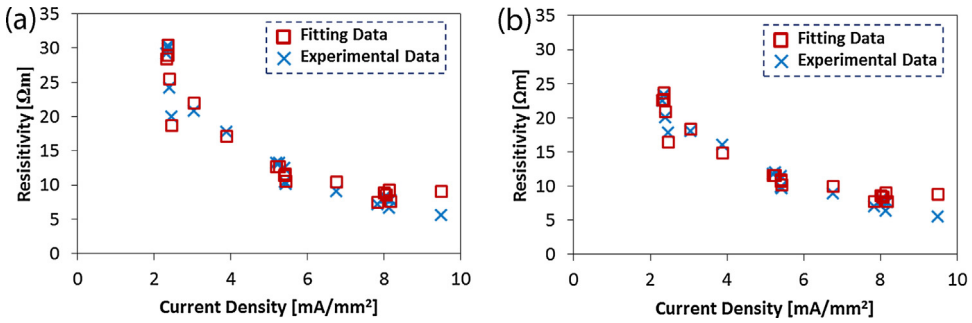

Fig. 9. Resistivity during FS calculated using the geometrical parameters of the specimens (a) and real resistivity estimated taking account of the porosity (b) as a function of the measured current density. The fitting data are calculated using Q = 0.94 eV, $\varepsilon = 0.65$ (a) and Q = 0.76 eV, $\varepsilon = 0.60$ (b) and provide good approximation to the experimental results.

(0.0092 Ωm). Fig. 9 shows the comparison between the experimental and the fitting results. One can observe that the model provides a satisfactory approximation of all measured parameters. Even changing the emissivity over a wide range (0.9–0.2), the activation energy varies between 0.87 and 0.95 eV. These values are slightly lower if compared to those previously measured in the experiments carried out using platinum electrodes (1.2–1.5 eV).

However, we also note that the samples during FS achieve different final densification and this affects the resistivity measurement. In other words, as the specimens treated with 2 mA/mm^2 are less dense than the others, the real current density is much higher than the "geometrical" value (calculated as the ratio between the current and the cross-section) and, therefore, the real resistivity of the material is lower than that previously estimated. It is possible to plot the real resistivity of the material (Fig. 9) if some hypotheses are accepted:

i The main part of densification occurs in the first minute after FS;
ii The specimen density can be approximated with the final density determined by Archimedes measurements;
iii The porosity is isotropic and homogeneously distributed.

Interpolation of the material resistivity data during FS was repeated by using the real resistivity values: the activation energy for conduction equal to 0.76 eV and an emissivity of 0.6 was estimated. In this case too, if the emissivity is varied between 0.2 and 0.9, the activation energy does not change significantly (0.71–0.77 eV). We note that the activation energy measured before FS using the power dissipation plot (1.2 eV) or the onset temperature for FS (1.5 eV) should not be affected by the presence of pores within the specimens, as the density of the green bodies is always the same. Therefore, the activation energy for electrical conduction undoubtedly decreases during FS. This conclusion is not straightforward; in fact, one must consider that upon FS the specimen temperature increases and this should yield to the activation of conduction mechanisms with higher energy barrier (if other conduction mechanisms are activated). Various reasons can be put forward for the observed discrepancy. Among them, the local physical/structural transformation at the grain boundary due to current concentration can very likely be considered fundamental, as the grain boundary is a preferential diffusion path [46], as pointed out in previous work. The hypothesized rearrangement of the grain boundary can also provide an explanation for rapid densification during FS, as other authors have proposed [1,19]. In addition, one can suggest that the lower densification observed when Ag electrodes are used can be accounted for by the lower specimen temperature, which does not strongly affect the grain boundary structure.

4. Conclusions

Uniaxially pressed samples made with nearly pure alumina powder can be flash sintered under electric fields in excess of 500 V/cm. Sintering temperatures significantly decrease with E-field to below 900 °C at 1500 V/cm. The current density is shown to be the main parameter controlling the sintering rate during flash sintering and the final density of the sintered bodies.

The conduction mechanism is complex and probably several phenomena are activated, although the evidence indicates a fundamental ionic contribution to conduction.

The model describing thermal runaway for flash sintering provides a good approximation of the correlation between the E-field and the onset temperature and indicates a conduction activation energy coherent with the other measurements.

The electrode material has a crucial effect on flash sintering, silver being very effective in reducing the sintering temperature in comparison with carbon or platinum.

The activation energy for conduction changes during the flash sintering phenomenon and this suggests local variation in the material structure, mainly associated with modification or structural rearrangement at the grain boundary.

References

[1] M. Cologna, B. Rashkova, R. Raj, Flash sintering of nanograin zirconia in <5 s at 850 °C, J. Am. Ceram. Soc. 93 (2010) 3556–3559.
[2] J.A. Downs, V.M. Sglavo, Electric field assisted sintering of cubic zirconia at 390 °C, J. Am. Ceram. Soc. 96 (2013) 1342–1344.
[3] J.S.C. Francis, Rishi Raj, Flash-sinterforging of nanograin zirconia: field assisted sintering and superplasticity, J. Am. Ceram. Soc. 95 (2012) 138–146.
[4] R.I. Todd, E. Zapata-Solvas, R.S. Bonilla, T. Sneddon, P.R. Wilshaw, Electrical characteristics of flash sintering: thermal runaway of Joule heating, J. Eur. Ceram. Soc. 35 (2015) 1865–1877.
[5] J.S.C. Francis, M. Cologna, R. Raj, Particle size effects in flash sintering, J. Eur. Ceram. Soc. 32 (2012) 3129–3136.
[6] R. Muccillo, E.N.S. Muccillo, An experimental setup for shrinkage evaluation during electric field-assisted flash sintering: application to yttria-stabilized zirconia, J. Eur. Ceram. Soc. 33 (2013) 515–520.
[7] R. Muccillo, M. Kleitz, E.N.S. Muccillo, Flash grain welding in yttria stabilized zirconia, J. Eur. Ceram. Soc. 31 (2011) 1517–1521.
[8] R. Baraki, S. Schwarz, O. Guillon, Effect of electrical field/current on sintering of fully stabilized zirconia, J. Am. Ceram. Soc. 95 (2012) 75–78.
[9] X. Hao, Y. Liu, Z. Wang, J. Qiao, K. Sun, A novel sintering method to obtain fully dense gadolinia doped ceria by applying a direct current, J. Power Sources 210 (2012) 86–91.
[10] R. Muccillo, E.N.S. Muccillo, M. Kleitz, Densification and enhancement of the grain boundary conductivity of gadolinium-doped barium cerate by ultra-fast flash grain welding, J. Eur. Ceram. Soc. 32 (2012) 2311–2316.
[11] E. Zapata-Solvas, S. Bonilla, P.R. Wilshaw, R.I. Todd, Preliminary investigation of flash sintering of SiC, J. Eur. Ceram. Soc. 33 (2013) 2811–2816.
[12] K.S. Naik, V.M. Sglavo, R. Raj, Flash sintering as a nucleation phenomenon and a model thereof, J. Eur. Ceram. Soc. 34 (2014) 4063–4067.
[13] K.S. Naik, V.M. Sglavo, R. Raj, Field assisted sintering of ceramic constituted by alumina and yttria stabilized zirconia, J. Eur. Ceram. Soc. 34 (2014) 2435–2442.

[14] Jesus Gonzalez-Julian, Olivier Guillon, Effect of electric field/current on liquid phase sintering, J. Am. Ceram. Soc. 98 (2015) 2018–2027.
[15] A. Gaur, V.M. Sglavo, Flash-sintering of $MnCo_2O_4$ and its relation to phase stability, J. Eur. Ceram. Soc. 34 (2014) 2391–2400.
[16] A.L.G. Prette, M. Cologna, V.M. Sglavo, R. Raj, Flash-sintering of Co_2MnO_4 spinel for solid oxide fuel cell applications, J. Power Sources 196 (2011) (2011) 2061–2065.
[17] A. Gaur, V.M. Sglavo, Flash sintering of (La, Sr)(Co, Fe)O_3-Gd-doped CeO_2 composite, J. Am. Ceram. Soc. 98 (2015) 1747–1752.
[18] A. Gaur, V.M. Sglavo, Densification of La0.6Sr0.4Co0.2Fe0.8O3 ceramic by flash sintering at temperature less than 100 °C, J. Mater. Sci. 49 (2014) 6321–6332.
[19] M. Cologna, J.S.C. Francis, R. Raj, Field assisted and flash sintering of alumina and its relationship to conductivity and MgO-doping, J. Eur. Ceram. Soc. 31 (2011) 2827–2837.
[20] R. Raj, M. Cologna, J.S.C. Francis, Influence of externally imposed and internally generated electrical fields on grain growth, diffusional creep sintering and related phenomena in ceramics, J. Am. Ceram. Soc. 94 (2011) 1941–1965.
[21] Y. Zhang, J. Jung, J. Luo, Thermal runaway, flash sintering and asymmetrical microstructural development of ZnO and ZnO–Bi_2O_3 under direct currents, Acta Mater. 94 (2015) 87–100.
[22] S.I. Bae, S. Baik, Determination of critical concentrations of silica and/or calcia for abnormal grain growth in alumina, J. Am. Ceram. Soc. 76 (1993) 1065–1067.
[23] I.J. Bae, S. Baik, Abnormal grain growth of alumina, J. Am. Ceram. Soc. 80 (1997) 1149–1156.
[24] C. Greskovich, J.A. Brewer, Solubility of magnesia in polycrystalline alumina at high temperatures, J. Am. Ceram. Soc. 84 (2001) 420–425.
[25] P. Boch, J.-C. Nièpce, Ceramic Materials: Processes, Properties and Applications, ISTE, Ltd, Chippenham, UK, 2007, pp. 200–205.
[26] N.D.M. Hine, K. Frensch, W.M.C. Foulkes, M.W. Finnis, A.H. Heuer, Bulk Diffusion in Alumina: Solving the Corundum Conundrum, 2009 (unpublished work) http://www.tcm.phy.cam.ac.uk/~mdt26/esdg_slides/hine030609.pdf.
[27] A. Tewari, U. Aschauer, P. Bowen, Atomistic modeling of effect of Mg on oxygen vacancy diffusion in α-alumina, J. Am. Ceram. Soc. 97 (2014) 2596–2601.
[28] K.P.D. Lagerlöf, R.W. Grimes, The defect chemistry of sapphire (α-Al_2O_3), Acta Mater. 46 (1998) 5689–5700.
[29] J. Pan, J. Öijerholm, A.B. Belonoshko, A. Rosengren, C. Leygraf, Self-diffusion activation energies in α-Al_2O_3 below 1000 °C—measurements and molecular dynamics calculation, Philos. Mag. Lett. 84 (2004) 781–789.
[30] Y. Oishi, W.D. Kingery, Self-Diffusion of oxygen in single crystal and polycrystalline aluminum oxide, J. Chem. Phys. 33 (1960) 480–486.
[31] J. Pappis, W.D. Kingery, Electrical properties of single-crystal and polycrystalline alumina at high temperatures, J. Am. Ceram. Soc. 44 (1961) 459–464.
[32] P.J. Harrop, Self-diffusion in simple oxides (a bibliography), J. Mater. Sci 3 (1968) 206–222.
[33] S.K. Mohapatra, F.A. Kroger, Defect structure of α-Al_2O_3 doped with magnesium, J. Am. Ceram. Soc. 60 (1977) 141–148.
[34] J. Öijerholm, J. Pan, C. Leygraf, In-situ measurements by impedance spectroscopy of highly resistive α-alumina, Corros. Sci. 48 (2006) 243–257.
[35] H.P.R. Frederikse, W.R. Hosler, High temperature electrical conductivity of aluminum oxide, Mater. Sci. Res. 9 (1975) 233–252, Mass Transport Phenomena in Ceramics.
[36] C. Barry Carter, M. Grant Norton, Ceramic Materials: Science and Engineering, Springer, 2007, pp. 532.
[37] H.A. Rahnamaye Alibad, S. Reza Ghorbani, Structural and spin polarization effects of Cr, Fe and Ti elements on electronical properties of α–Al_2O_3 by first principle calculations, J. Mod. Phys. 2 (2011) 158–161.
[38] H.A. Rahnamaye Aliabad, M.R. Benam, H. Arabshahi, Theoretical studies of the effect of Ti, Zr and Hf substitutions on the electronic properties of alpha alumina, Int J. Phys. Sci. 4 (2009) 437–442.
[39] A.F. Lima, J.M. Dantas, M.V. Lalic, An ab-initio study of electronic and optical properties of corundum Al2O3 doped with Sc, Y, Zr and Nb, J. Appl. Phys. 112 (2012).
[40] I. Costina, R. Franchy, Band gap of amorphous and well-ordered Al_2O_3 on Ni_3Al (100), Appl. Phys. Lett. 78 (2001) 4139–4141.
[41] R.J. Brook, J. Yee, F.A. Kroeger, Electrochemical cells and electrical conduction of pure and doped Al_2O_3, J. Am. Ceram. Soc. 54 (1971) 444–451.
[42] H.M. Kizillyalli, P.R. Mason, DC and AC electrical conduction in single crystal alumina, Phys. Stat. Sol. (a) 36 (1976) 499–508.
[43] K. Kitazawa, R.L. Coble, Chemical diffusion in polycrystalline Al_2O_3 as determined from electrical conductivity measurements, J. Am. Ceram. Soc. 57 (1974) 250–253.
[44] K. Kitazawa, R.L. Coble, Electrical conduction in single-crystal and polycrystalline Al_2O_3 at high temperatures, J. Am. Ceram. Soc. 57 (1974) 245–250.
[45] A.H. Heuer, Oxygen and aluminum diffusion in α-Al_2O_3: how much do we really understand? J. Am. Ceram. Soc 28 (2008) 1495–1507.
[46] A.E. Paladino, R.L. Coble, Effect of grain boundaries on diffusion-controlled processes in aluminum oxide, J. Am. Ceram. Soc. 46 (1963) 133–136.
[47] T. Nakagawa, I. Sakaguchi, N. Shibata, K. Matsunaga, T. Mizoguchi, T. Yamamoto, H. Haneda, Y. Ikuhara, Yttrium doping effect on oxygen grain boundary diffusion in α-Al_2O_3, Acta Mater. 55 (2007) 6627–6633.
[48] N.M. Tallan, H.C. Graham, Interfacial polarization and electrical conductivity in sapphire, J. Am. Ceram. Soc. 48 (1965) 512–516.
[49] J.H. Harding, Experiment and theory of diffusion in alumina, J. Am. Ceram. Soc. 86 (2003) 554–559.
[50] P.W.M. Jacobs, E.A. Kotomin, Defect energies for pure corundum and for corundum doped with transition metal ions, Philos. Mag. A 68 (1993) 695–709.
[51] Y. Oishi, K. Ando, Y. Kubota, Self-diffusion of oxygen in single crystal alumina, J. Chem. Phys. 73 (1980) 1410–1412.
[52] D. Martin, D. Duprez, Mobility of Surface Species on Oxides. 1. Isotopic Exchange of ^{18}Mobility of surface species on oxides. 1. Isotopic exchange of $^{18}O_2$ with ^{16}O of SiO_2, Al_2O_3, ZrO_2, MgO, CeO_2 and CeO_2-Al_2O_3. Activation by noble metals. Correlation with oxide basicity, J. Phys. Chem. 100 (1996) 9429–9438.
[53] W. Shin, W.-S. Seo, K. Koumoto, Grain-boundary grooves and surface diffusion in polycrystalline alumina measured by atomic force microscope, J. Eur. Ceram. Soc. 18 (1998) 595–600.
[54] L. Badrour, E.G. Moya, J. Bernardini, F. Moya, Fast diffusion of silver in single and polycrystals of α-alumina, J. Phys. Chem. Solids 50 (1989) 551–561.
[55] E.G. Gontier-Moya, J. Bernardini, F. Moya, Silver and platinum diffusion in alumina single crystals, Acta Mater. 49 (2001) 637–644.
[56] M.N. Avadhanulu, P.G. Kshirdagar, A Textbook of Engineering Physics, S. Chand & Co. Ltd., New Delhi, India, 2013, pp. 346.
[57] D.R. Lide, Handbook of Chemistry and Physics, CRC Press, 2004, pp. 12–124.